Chem
Europ
European O
Societies P

Check for
updates

Cycloaddition

Mechanism and Regioselectivity of Intramolecular [2+2] Cycloaddition of Ene–Ketenes: A DFT Study

Xing Fan,[a] Pan Zhang,[a] Yi Wang,[a] and Zhi-Xiang Yu*[a]

Abstract: Intramolecular [2+2] cycloaddition of ene–ketenes gives either fused-ring (via normal [2+2] cycloaddition) or bridged-ring (via cross-[2+2] cycloaddition) cyclobutanones. For example, terminal ene–ketenes give the fused-ring cycloadducts, whereas dimethyl-substituted ene–ketenes furnish bridged-ring cycloadducts. For monomethyl-substituted ene–ketenes, both [2+2] cycloadducts are generated. However, there are no systematic theoretical studies on such regiochemistry in the literature. Herein, we report our DFT study on the mechanism and regioselectivity of these intramolecular [2+2] cycloadditions. DFT calculations reveal that both normal and cross-[2+2] cycloadditions are concerted processes. The normal [2+2] cycloaddition transition state is forming an internal carbocation while the cross-[2+2] cycloaddition transition state is generating an external carbocation (see Scheme 1 of the paper). On the basis of the relative stability of these carbocations, which is affected by both the tether and the substituent(s) on the alkene, a regiochemistry prediction model is proposed to understand and predict the reaction outcome.

Introduction

[2+2] cycloaddition of ketenes and alkenes is one of the most powerful reactions for cyclobutanone synthesis.[1] This reaction, which is one of the so-called Staudinger ketene cycloadditions, has been widely used in the total synthesis of natural products.[2] In addition, the resulting cyclobutanone products and their derivatives (for example, cyclobutanols) have been used as substrates in transition-metal-catalyzed C–C bond activation reactions.[3] The [2+2] cycloaddition of ketenes with alkenes, which is close to the symmetry-forbidden [2+2] cycloaddition of two alkenes in terms of the reaction format, was regarded as an exception to the Woodward–Hoffmann rules.[4] Due to this, intensive studies on the mechanism of [2+2] cycloaddition of ketenes and alkenes have been carried out.[4] Now it is accepted that this [2+2] cycloaddition is concerted and starts from the interaction between alkene's HOMO and ketene's LUMO (Figure 1). The secondary orbital interaction between ketene's π(C=C) orbital and alkene's LUMO has been used to explain why a perpendicular transition state is required for the intermolecular [2+2] cycloaddition. The proposed orbital interaction for this symmetry-allowed reaction is $[_\pi 2_s + (_\pi 2_s + _\pi 2_s)]$.[4c,4d] Charge separation model was also proposed to account for the regioselectivity.[4f] Recently, Lewis-acid-catalyzed intermolecular [2+2] cycloaddition of ketenes and alkenes have also been developed[1d] and its mechanism has been investigated.[4h]

[a] X. Fan, P. Zhang, Dr. Y. Wang, Prof. Dr. Z.-X. Yu
Beijing National Laboratory for Molecular Sciences (BNLMS),
Key Laboratory of Bioorganic Chemistry and Molecular Engineering
of Ministry of Education, College of Chemistry, Peking University,
Beijing 100871, China
E-mail: yuzx@pku.edu.cn
https://www.chem.pku.edu.cn/zxyu/index/index.htm
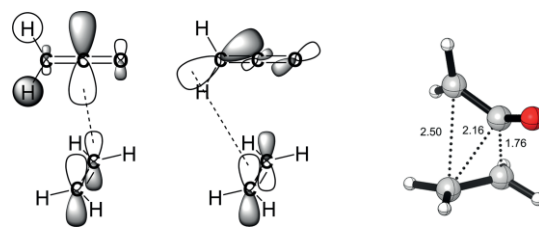
Figure 1. The main (left) and secondary (middle) orbital interactions between ketene and alkene and the [2+2] cycloaddition transition state (right).

Some examples for intramolecular [2+2] cycloaddition of ketenes (and keteniminium salts, which are not discussed in this work) with alkenes are shown in Table 1.[5] Two types of intramolecular [2+2] cycloadducts could be obtained, depending on the substitution pattern of the ene–ketene substrates, which were in situ generated from acyl chlorides. One type is the normal [2+2] cycloaddition that gives bicyclic 5/4 products (bicyclic 6/4 products can also be formed by using elongated substrates). The other type is the cross-[2+2] cycloaddition, giving rise to the bridged-ring products. Similar intramolecular [2+2] cycloaddition of ene–ketenimines, which were in situ generated from 1,6-enynes, was also reported.[6] Other intramolecular [2+2] cycloadditions of ketenes have been developed, including the intramolecular [2+2] cycloaddition of in situ generated ketenes from alkynyl ethers and cyclobutenones[7] and the intramolecular [2+2] cycloaddition of ketenes with allenes.[8]

Previous theoretical studies have been focused on the intermolecular [2+2] cycloaddition of ketenes with alkenes. However, for intramolecular [2+2] cycloaddition of ene–ketenes,[9] no systematic theoretical rationale for the regioselectivity has been reported, which is now disclosed in this paper.

Table 1. Intramolecular [2+2] cycloaddition of ene–ketenes (precursors can be found in the original reports).

Results and Discussion

In this part, we will first discuss the detailed mechanism of the intramolecular [2+2] cycloaddition of ene–ketene **1** (Figure 2). A regiochemistry prediction model will also be presented. Then, by applying this model, we will discuss how substituents affect the regiochemistry (normal vs. cross-[2+2] cycloadditions). After that, more examples will be elaborated to discuss whether other ene–ketene substrates with different tethers follow the regiochemistry prediction model.
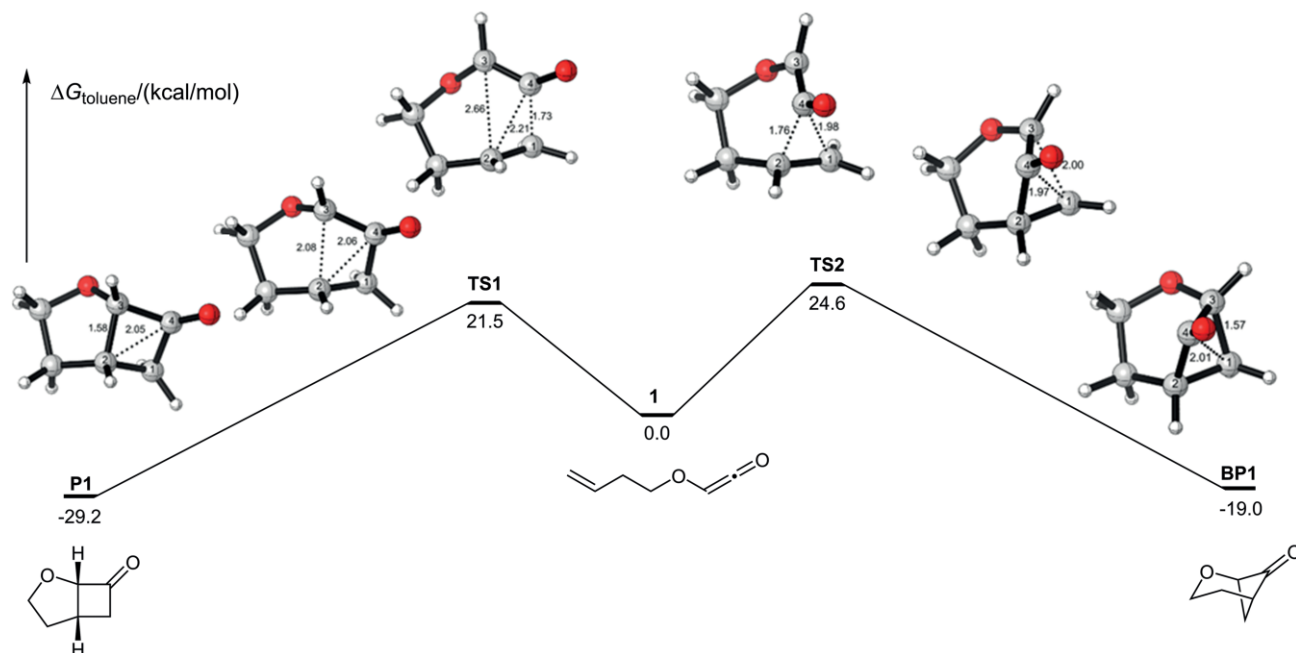
Figure 2. DFT-computed free energy surface of [2+2] cycloadditions of ene–ketene **1** and selected structures from IRC calculations.

EurJOC
European Journal of Organic Chemistry

Full Paper
doi.org/10.1002/ejoc.202001007

Chemistry Europe
European Chemical
Societies Publishing

Mechanism and Regiochemistry of the Reaction of Ene–Ketene 1

The free energy surface of two types of [2+2] cycloaddition of terminal ene–ketene **1** is shown in Figure 2. Ene–ketene **1** undergoes the normal [2+2] cycloaddition via **TS1** with an activation free energy of 21.5 kcal/mol, leading to fused-ring cyclobutanone **P1**. This normal [2+2] cycloaddition is exergonic by 29.2 kcal/mol. In **TS1**, the C1–C4 bond is partially formed with a bond length of 1.73 Å, while the C2–C3 bond with a bond length of 2.66 Å is far from generated. Intrinsic reaction coordinate (IRC) calculations showed that **TS1** directly leads to the [2+2] cycloadduct and the formation of C1–C4 bond is much earlier than the formation of C2–C3 bond (Figure 2). Therefore, this [2+2] cycloaddition is concerted but asynchronous (see Supporting Information for discussion on disfavored diradical stepwise mechanism). The dihedral angle of C2–C1–C4–C3 in **TS1** is 68°, while the corresponding value of the intermolecular [2+2] cycloaddition transition state is 62° (Figure 1). The present [2+2] cycloaddition is similar to carbonyl–ene and Prins reactions because all of them involve the nucleophilic attack of alkenes to carbonyl groups.[10]

In **TS1**, the terminal carbon (C1) of the alkene is forming a C–C bond with C4, and the internal carbon (C2) has some characters of a carbocation (see Supporting Information for the charge distribution of the substrate and transition states). **TS1** gradually becomes a temporary internal carbocation at C2 (see results from IRC calculations in Figure 2). Therefore, we can use the relative stability of C2-carbocation, the internal carbocation in **TS1**, to understand the relative ease of the normal [2+2] cycloadditions (Scheme 1).

Alternatively, ene–ketene **1** may undergo cross-[2+2] cycloaddition via **TS2**, requiring an activation free energy of 24.6 kcal/mol. This cycloaddition gives bridged-ring cyclobutanone **BP1** and is exergonic by 19.0 kcal/mol. In **TS2**, the C2–C4 bond is 1.76 Å, and the C1–C4 bond is 1.98 Å, which is much shorter than the C1–C3 bond. IRC calculations gave results similar to those of the normal [2+2] cycloaddition. In **TS2**, C2–C4 bond is forming and C1 is becoming a carbocation (Scheme 1). Here we label this carbocation as an external carbocation. The stability of this external carbocation affects the reaction outcome.

The above calculations suggest that the normal [2+2] cycloaddition of **1** is favored over the cross-[2+2] cycloaddition by 3.1 kcal/mol, which agrees with the experimental observation (Table 1).[5b] This can be understood by considering the relative stability of the internal carbocation in **TS1** with respect to the external carbocation in **TS2**. Here the internal carbocation is a secondary carbocation while the external carbocation is a primary one. Therefore, **TS1** is favored over **TS2**.

Frontier Molecular Orbital (FMO) Analysis

FMO analysis shows that the HOMO–1 orbital is mainly the π orbital of alkene, while the LUMO orbital mainly consists of the π*(C=O) orbital of ketene (Figure 3). During the [2+2] cycloaddition, HOMO–1 interacts with LUMO, namely, the π orbital of alkene interacts with the π*(C=O) orbital of ketene, which
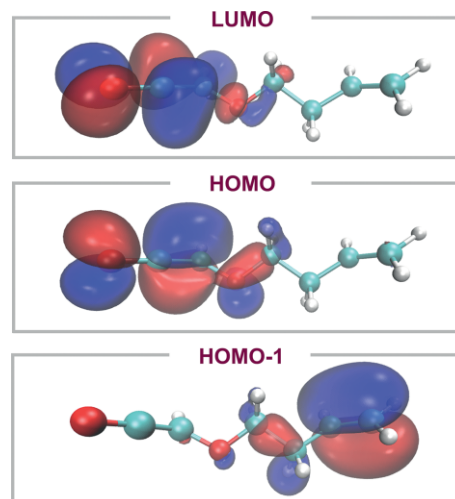
Figure 3. Frontier molecular orbitals of ene–ketene **1**.
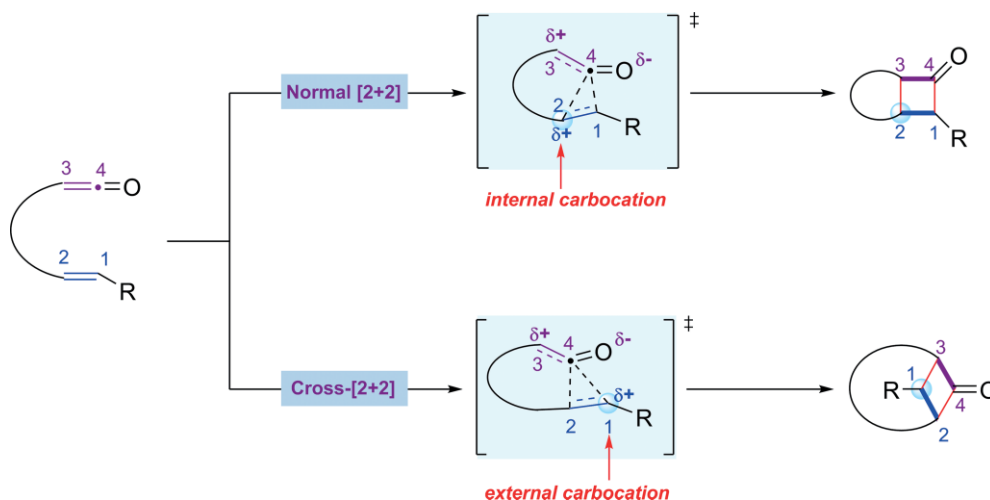
Scheme 1. Rationale for the regioselectivity of intramolecular [2+2] cycloadditions of ene–ketenes.

EurJOC
European Journal of Organic Chemistry

Full Paper
doi.org/10.1002/ejoc.202001007

Chemistry
Europe
European Chemical
Societies Publishing

resembles that of the intermolecular [2+2] cycloaddition (Figure 1).

Substituent Effect on the [2+2] Cycloaddition of Ene–Ketenes

In this part, we will present more examples to understand how substituents affect the regiochemistry of the intramolecular [2+2] cycloaddition of ene–ketenes by using the relative stability of the internal vs. external carbocations in the transition states (Scheme 1).

a) Internal substituted ene–ketene 2. Here our model suggests that if an internal substitution is introduced, the internal cation will be further stabilized and the normal [2+2] cycloaddi-

tion will be facilitated. This is the case of substrate **2**, showing that normal [2+2] cycloaddition is favored over the cross-[2+2] cycloaddition by 2.4 kcal/mol (Figure 4). In the normal [2+2] cycloaddition pathway, the reaction of **2** is easier than that of **1** by 3.0 kcal/mol (**2**: 18.5 vs. **1**: 21.5 kcal/mol) because the 1,1-disubstituted alkene of **2** is more nucleophilic than the mono-substituted alkene of **1**. Experimentally, the reaction yields of substrates **1** and **2** were 16 % and 72 %, respectively.[5b] We had speculated that the low yield of substrate **1** could originate from the competition of the ketene dimerization. However, when we repeated the experiments, we did not observe the dimerized products (see Supporting Information for details). The poor reactivity of **1** and the presence of other side reactions may lead to the low reaction yield.
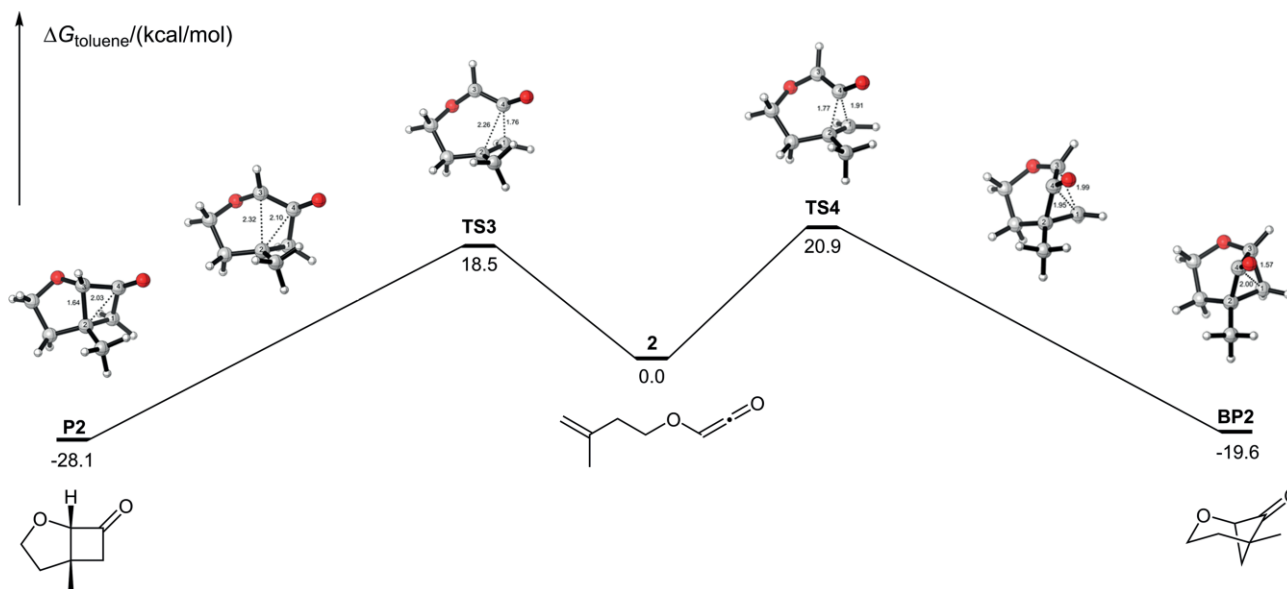
Figure 4. DFT-computed free energy surface of [2+2] cycloadditions of ene–ketene **2**.
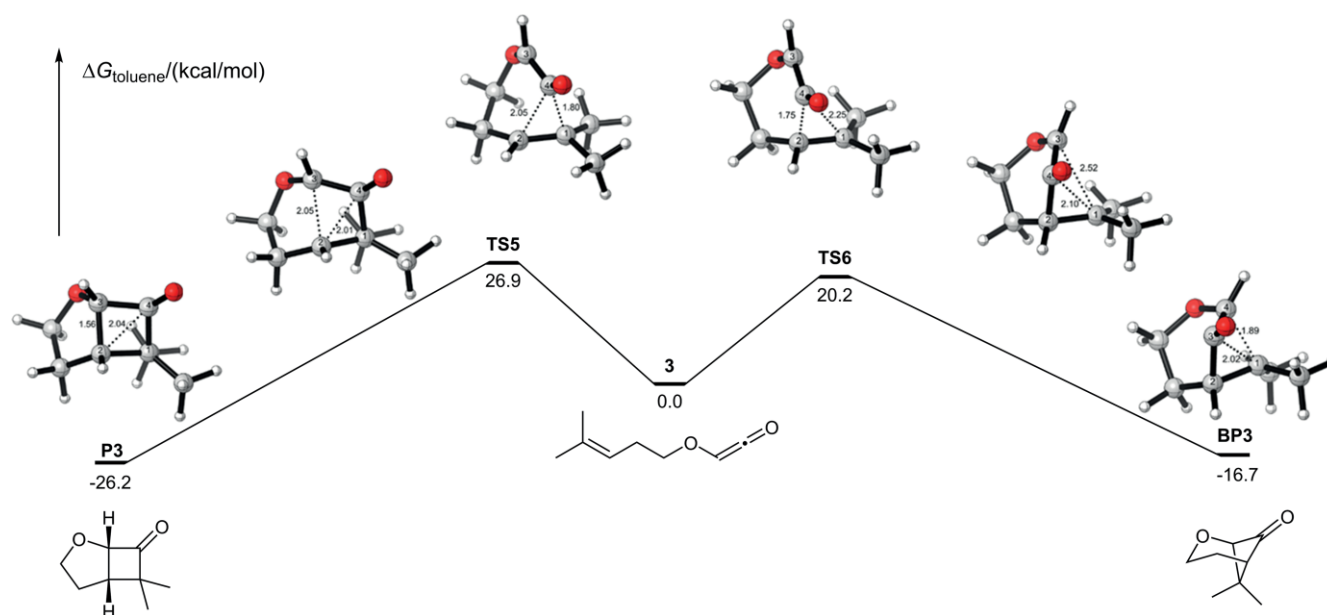
Figure 5. DFT-computed free energy surface of [2+2] cycloadditions of ene–ketene **3**.

EurJOC
European Journal of Organic Chemistry

Full Paper
doi.org/10.1002/ejoc.202001007

Chemistry
Europe
European Chemical
Societies Publishing

b) Dimethyl-substituted ene–ketene 3. The free energy surface of the [2+2] cycloadditions of dimethyl-substituted ene–ketene **3** is shown in Figure 5. DFT calculations suggested that **3** may undergo normal [2+2] cycloaddition via **TS5** with an activation free energy of 26.9 kcal/mol. This reaction provides fused-ring cyclobutanone **P3** and is exergonic by 26.2 kcal/mol. Alternatively, **3** may also undergo cross-[2+2] cycloaddition via **TS6**, which requires an activation free energy of 20.2 kcal/mol. This step provides bridged-ring cyclobutanone **BP3** and is exergonic by 16.7 kcal/mol. Different from the reaction of **1**, **TS5** in the normal [2+2] cycloaddition pathway is disfavored over **TS6** in the cross-[2+2] cycloaddition pathway by 6.7 kcal/mol, suggesting that the bridged-ring cycloadduct **BP3** should be the major product in this case. This can be understood by using Scheme 1, considering that the generated tertiary external carbocation in the cross-[2+2] cycloaddition transition state **TS6** is more stable than the secondary internal carbocation in the transition state of the normal [2+2] cycloaddition (**TS5**). Therefore, cross-[2+2] cycloaddition should be preferred, which is consistent with the experimental observation (Table 1).[5b]

c) Monomethyl-substituted ene–ketene 4. The free energy surface of monomethyl-substituted ene–ketene **4** is depicted in Figure 6 (the experimentally used ethyl group[5d] is simplified as a methyl group here). Similarly, monomethyl-substituted ene–ketene **4** may undergo normal [2+2] cycloaddition via **TS7** with an activation free energy of 21.2 kcal/mol, which leads to fused-ring cyclobutanone **P4**. Alternatively, **4** may also proceed through the cross-[2+2] cycloaddition via **TS8** with an activation free energy of 21.3 kcal/mol, which forms bridged-ring cyclobutanone **BP4**. **TS7** and **TS8** are nearly isoenergetic, suggesting that both cycloadducts should be generated, which accords with the experimental observation (Table 1). Considering

that both pathways lead to secondary carbocations (stabilized by the tether and the methyl group, respectively) in their transition states, the difference between the internal and external carbocations is small in terms of stability (Scheme 1). Consequently, the regioselectivity of substrate **4** is expected to be low.

d) Vinyl-substituted ene–ketene 5. Here we discuss the reaction of ene–ketene **5** to understand how vinyl group affects the competition of the normal and cross-[2+2] cycloadditions (Figure 7). According to the model shown in Scheme 1, we predict that the cross-[2+2] cycloaddition should be favored over the normal one because the vinyl group stabilizes the carbocation in the transition state better than the tether does. This is supported by our DFT calculations, showing that **TS10** in the cross-[2+2] cycloaddition pathway is favored over **TS9** in the normal [2+2] cycloaddition pathway by 1.4 kcal/mol. Interestingly, **BP5** may undergo retro-Claisen rearrangement via **TS12**, requiring an activation free energy of 36.1 kcal/mol. The retro-Claisen rearrangement leads to the formation of a 6/6 fused-ring product **CP** and this step is exergonic by 5.8 kcal/mol. Therefore, the reaction of **5** should give **CP** and this is consistent with the experimental observation.[5d] The formation of **CP** from **5** may also result from a concerted [4+2] cycloaddition via **TS11**. We find that this pathway has a similar activation free energy with that of the cross-[2+2] cycloaddition, suggesting that both pathways may lead to the formation of **CP**.

e) Cycloalkene–ketene 6. If the alkene moiety of the substrate is a cycloalkene, the regiochemistry can also be explained by our model (Scheme 1). Taking substrate **6** as an example, we predict that the normal [2+2] cycloaddition should be favored because its transition state **TS13** possesses a tertiary internal carbocation, whereas the cross-[2+2] cycloaddition transition state **TS14** has a secondary external carbocation (Figure 8). DFT
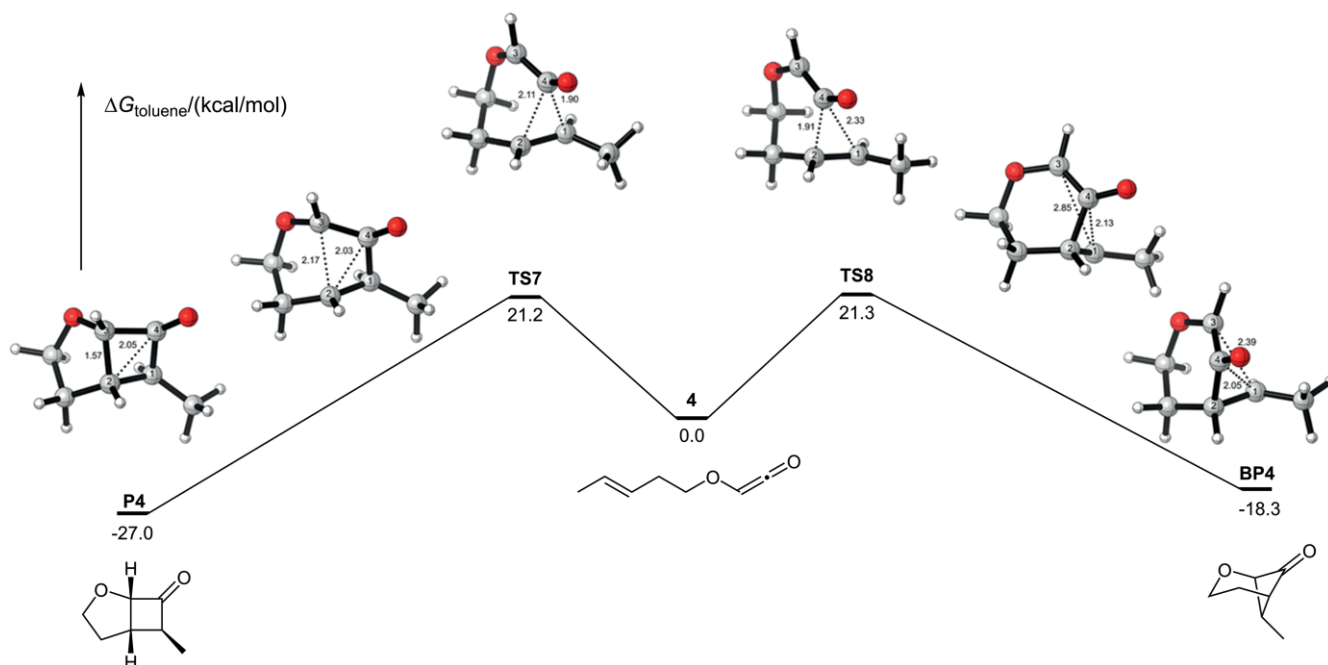
Figure 6. DFT-computed free energy surface of [2+2] cycloadditions of ene–ketene **4**.

EurJOC
European Journal of Organic Chemistry

Full Paper
doi.org/10.1002/ejoc.202001007

**Chemistry
Europe**
European Chemical
Societies Publishing
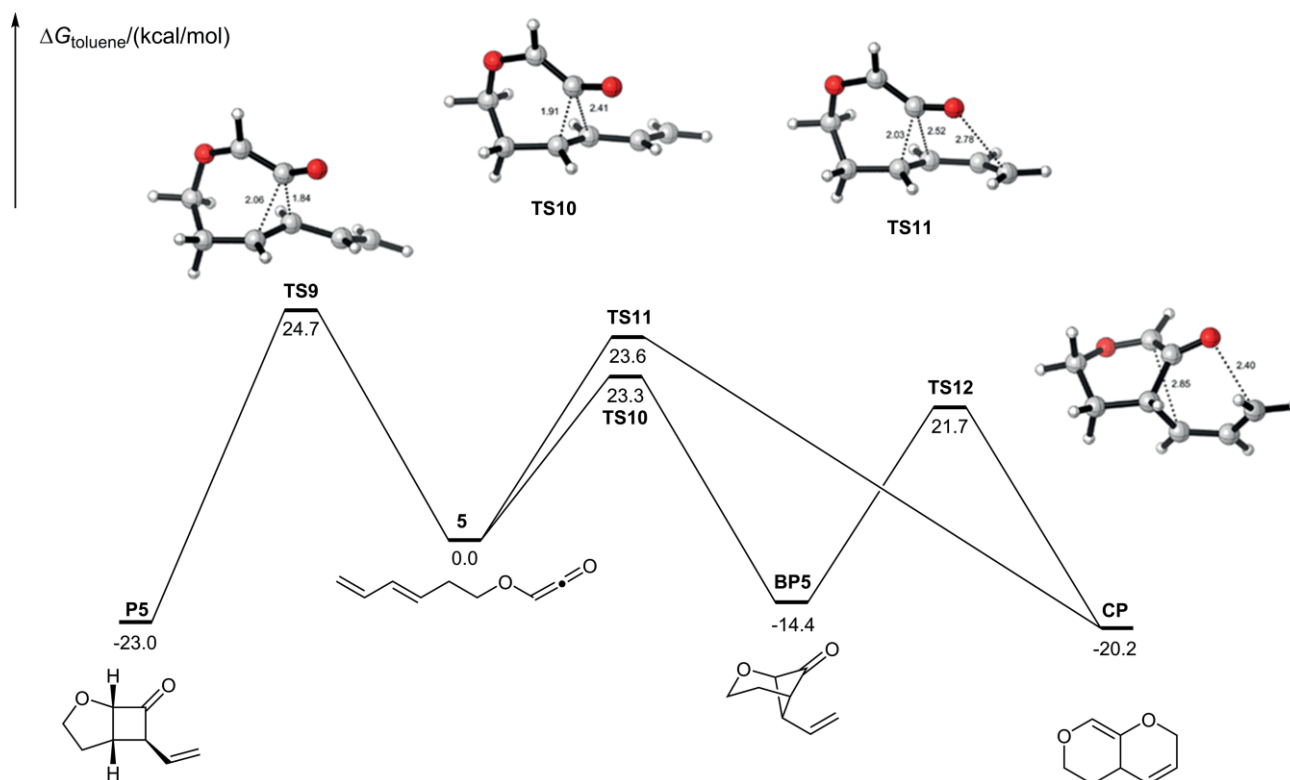
Figure 7. DFT-computed free energy surface of [2+2] cycloadditions of ene–ketene **5**.

calculations supported this, showing that **TS13** is favored over **TS14** by 1.3 kcal/mol, which agrees with the experimental observation that the normal [2+2] cycloadduct **P6** was obtained as the major product.[5c]
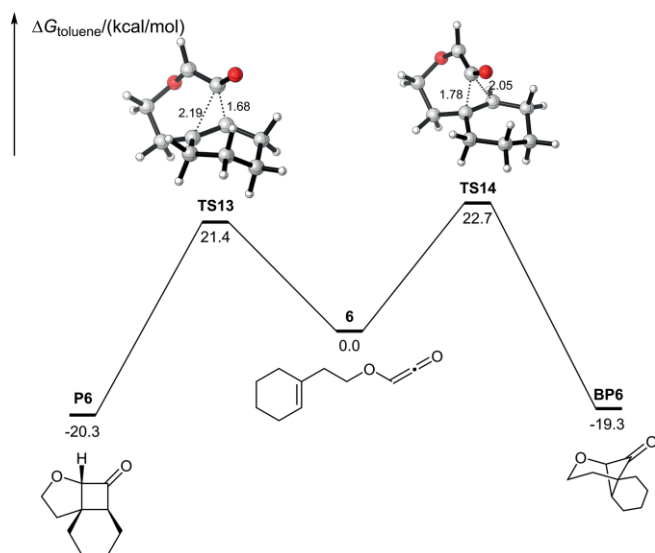
Figure 8. DFT-computed free energy surface of [2+2] cycloadditions of ene–ketene **6**.

f) Summary of the substituent effect and the regiochemistry prediction model. For terminal ene–ketenes, the internal carbocation in the normal [2+2] cycloaddition transition state is a secondary carbocation and is more stable than the primary

external carbocation in the cross-[2+2] cycloaddition transition state. Consequently, the normal [2+2] cycloaddition takes place. If an alkyl group is introduced to the internal position of the alkene, normal [2+2] cycloaddition is also favored over the cross-[2+2] cycloaddition because the internal cabocation is now tertiary while the external carbocation is still primary. For ene–ketenes with two substituents at the terminal position, the external carbocation in the cross-[2+2] cycloaddition transition state is a tertiary carbocation, which is more stable than the secondary internal carbocation in the normal [2+2] cyclo-addition. Therefore, disubstituted ene–ketenes prefer to give cross-[2+2] cycloadducts. For ene–ketenes with only one alkyl substituent at the terminal position, the internal and external carbocations in the transition states are both secondary carbo-cations and have similar stabilities. Consequently, both pathways can take place and a mixture of two cycloadducts is generated.

Therefore, the relative stability of internal vs. external carbocations in the transition states can be used as a guiding principle to understand and predict the regiochemistry (Scheme 1). This model can also be applied to some ene–ketene substrates with different tethers (vide infra). It is worth mentioning that our regiochemistry prediction model is based on kinetics and all of the discussed reactions in this paper, expect for one substrate, **16** (vide infra), are regarded as kinetically controlled reactions, considering that their reverse reactions have computed activation free energies of more than 35 kcal/mol. We also point out that the interconversion of normal and cross-[2+2] cyclo-adducts is not possible due to very high barrier involved (see Supporting Information for details).

EurJOC
European Journal of Organic Chemistry

Full Paper
doi.org/10.1002/ejoc.202001007

Chemistry Europe
European Chemical Societies Publishing

Application of the Regiochemistry Prediction Model to Carbon-Tethered Ene–Ketenes

In reactions discussed above, each substrate has an oxygen tether. In fact, our regiochemistry prediction model can also be applied to carbon-tethered ene–ketenes. As depicted in Scheme 2, several experimental results are chosen to test the regiochemistry prediction model. Based on our model, both reactions of **7** and **8** should give normal [2+2] cycloadducts because secondary and tertiary internal carbocations will be generated in the normal [2+2] cycloaddition transition states, respectively, while the cross-[2+2] cycloadditions generate primary external carbocations. DFT calculations supported these predictions, showing that normal [2+2] cycloaddition transition states are favored over the cross-[2+2] cycloaddition transition states.
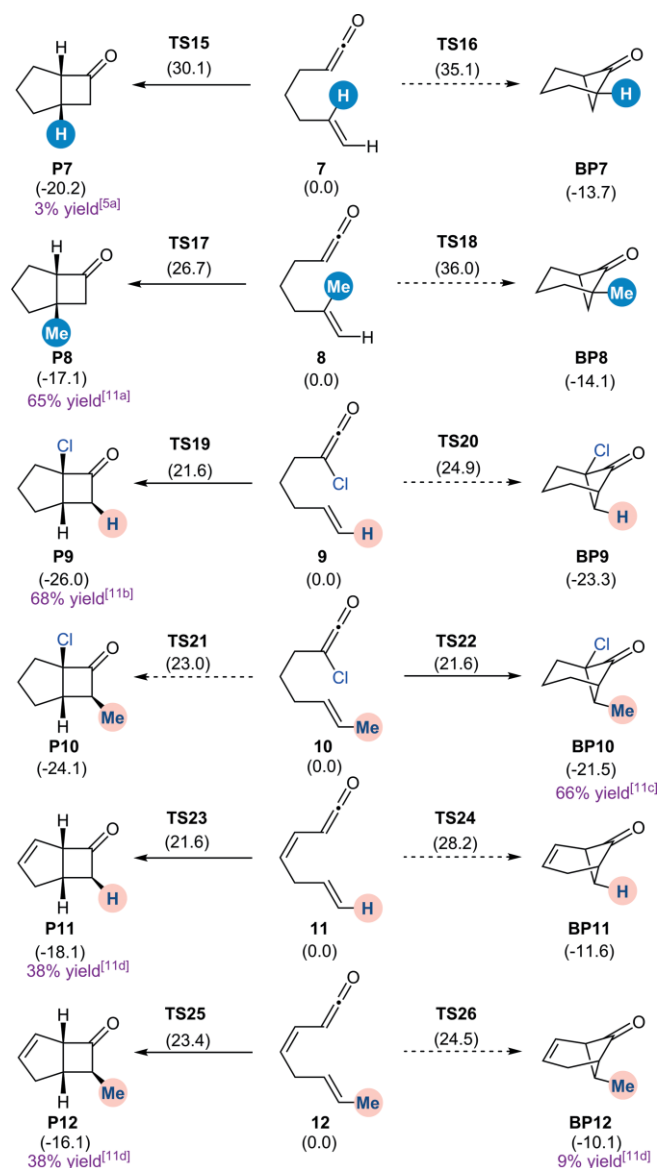
Scheme 2. DFT-computed pathways and the reaction outcome of several [2+2] cycloadditions. Free energies are reported in kcal/mol.

Experimentally, the yield of **P7** was low possibly due to the dimerization of **7**.[5a] DFT calculations indicated that the activa-

tion free energy of the dimerization is 27.5 kcal/mol (see Supporting Information for details), which is 2.6 kcal/mol lower than the normal [2+2] cycloaddition (30.1 kcal/mol). As a result, the [2+2] cycloaddition becomes the side reaction and the reaction may mainly give the dimerized product.

As compared with the reaction of substrate **1**, the normal [2+2] cycloaddition of substrate **7** is much more difficult (**7**: 30.1 kcal/mol vs. **1**: 21.5 kcal/mol). Two reasons account for this. The first one is that the oxygen atom of the tether decreases the LUMO energy (**1**: –2.2 eV vs. **7**: –1.0 eV; computed at the B3LYP/def2-SVP level), which consequently increases the electrophilicity of the ketene. On the other hand, the oxygen atom may afford the extra Thorpe–Ingold effect to promote the cyclization.[12]

For substrate **8**, the normal [2+2] cycloaddition has an improved yield of 65 %.[11a] This can be understood by our computational results. The normal [2+2] cycloaddition of **8** (26.7 kcal/mol) is easier than that of **7** (30.1 kcal/mol), suggesting that the dimerization process (with an activation free energy of ca. 27.5 kcal/mol, estimated from the dimerization of **7**) becomes disfavored.

As predicted by our model, the reaction of **9** should give the normal [2+2] cycloadduct **P9** whereas the reaction of **10** should give both cycloadducts **P10** and **BP10**. DFT calculations supported the former one but not the latter one (Scheme 2). We suggest that the Cl and O atoms experience steric repulsions in the cycloaddition transition states. The repulsion is more severe in **TS21** than in **TS22**, as can be appreciated by the Cl–O distance of 3.08 (**TS21**) and 3.12 Å (**TS22**), respectively (see Supporting Information for details). Consequently, the steric effect overrides the relative stability of internal and external carbocations. The reactions of substrates **9** and **10** are easier than those of **7** and **8** because ketenes with Cl substituents are more reactive.

We have also studied the reactions of **11** and **12** with a double bond in the tether. The normal [2+2] cycloaddition pathway of **11** is favored over the cross-[2+2] cycloaddition pathway by 6.6 kcal/mol, which is consistent with our model and the experimental result.[11d] A mixture was obtained for **12**, which is similar to **4**. As DFT calculations predicted, the yield of **P12** is higher than that of **BP12**.

Application of the Regiochemistry Prediction Model to Arene-Tethered Ene–Ketenes

Our model can also be applied to arene-tethered ene–ketenes (Figure 9). In these cases, the secondary internal carbocation can be further stabilized by the arene tether and the preference to the normal [2+2] cycloaddition can be further enhanced. For example, the normal [2+2] cycloaddition of **13** requires an activation free energy which is 2.7 kcal/mol lower than that of the cross-[2+2] cycloaddition (Figure 9a). For substrate **14** with a terminal methyl group, even though the external carbocation is stabilized by the methyl group, the stabilization effect of the arene tether on the internal carbocation is more significant (Figure 9b). Therefore, **14** also prefers the normal [2+2] cycloaddition. Here we point out that the [2+2] cycloadduct **P14** can

EurJOC
European Journal of Organic Chemistry

Full Paper
doi.org/10.1002/ejoc.202001007

**Chemistry
Europe**
European Chemical
Societies Publishing
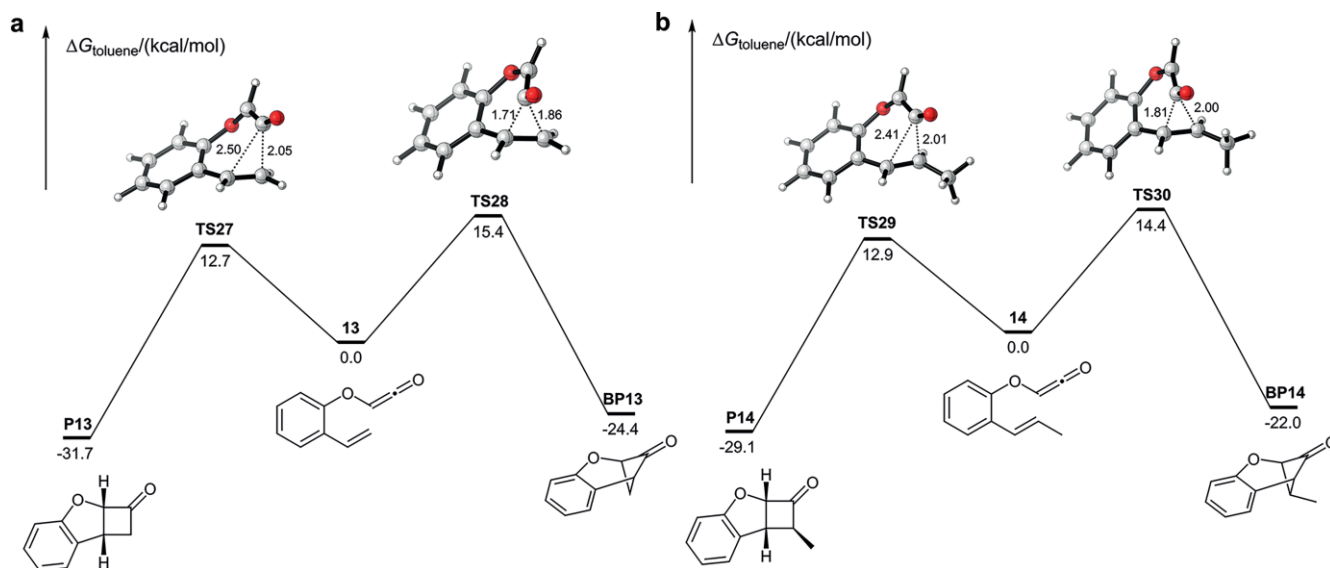
Figure 9. DFT-computed free energy surfaces of [2+2] cycloadditions of ene–ketenes **13** and **14**.

then undergo an isomerization to give a diastereomeric mixture, as observed experimentally (Table 1).[5e]

One Variation from the Regiochemistry Prediction Model: The Regiochemistry of Imine-Tethered Ene–Ketenes Could Be Controlled by Thermodynamics

Our regiochemistry prediction model is based on kinetics, suggesting that it may not be applied to thermodynamically controlled reactions.

For imine-tethered substrate **15**, the normal [2+2] cycloaddition via **TS31** is favored over the cross-[2+2] cycloaddition via

TS32 by 4.3 kcal/mol (Figure 10**a**), suggesting that only the normal [2+2] cycloadduct should be observed experimetally. Indeed, normal [2+2] cycloadduct **P15** was obtained in 62 % yield.[5g] This is consistent with our model considering that there is no substitution on the alkene part.

In contrast, for substrate **16** with a terminal methyl group (Figure 10**b**), a mixture of normal and cross-[2+2] cycloadducts should be obtained according to our regiochemistry prediction model (Scheme 1). Experimentally, the normal [2+2] cycloadduct **P16** was obtained in 46 % yield and no cross-[2+2] cycloadduct **BP16** was observed. Our DFT calculations indicated that the cross-[2+2] cycloaddition via **TS34** is kinetically favored over
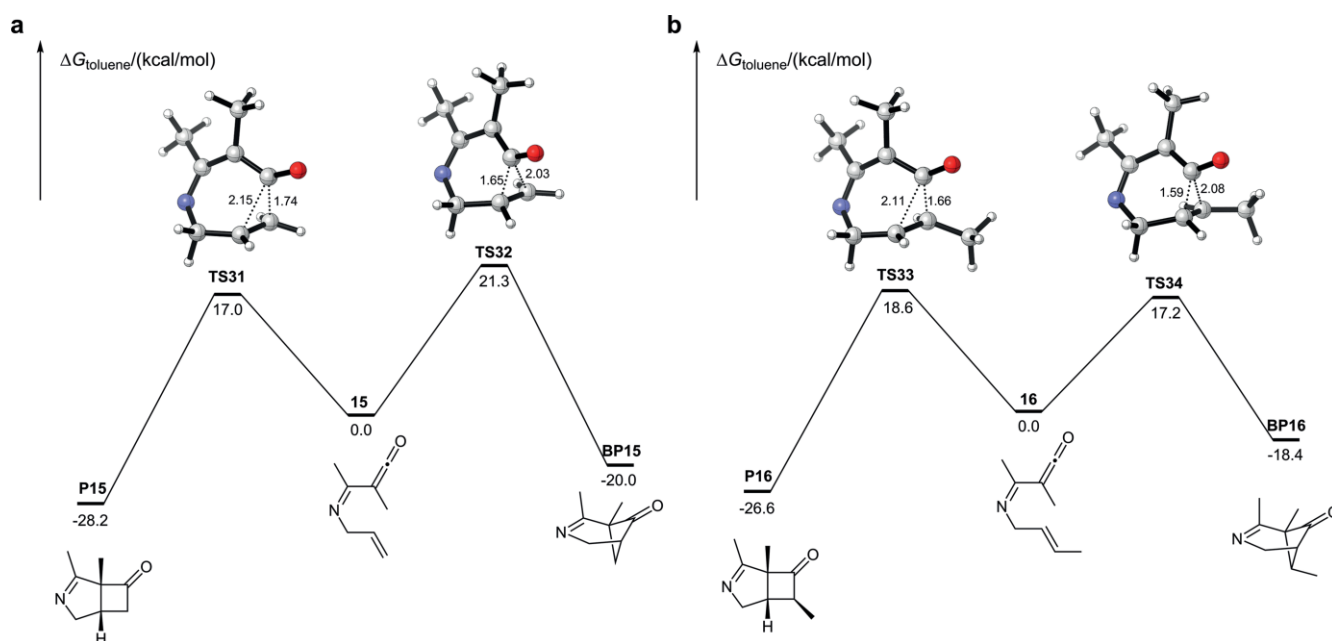
Figure 10. DFT-computed free energy surfaces of [2+2] cycloadditions of imine-tethered ene–ketenes **15** and **16**.

EurJOC
European Journal of Organic Chemistry

Full Paper
doi.org/10.1002/ejoc.202001007

**Chemistry
Europe**
European Chemical
Societies Publishing

the normal [2+2] cycloaddition via **TS33** by 1.4 kcal/mol. But this reaction can be regarded as a thermodynamically-controlled reaction because the reverse reaction in the cross-[2+2] cycloaddition pathway with an activation free energy of 35.6 kcal/mol is not difficult under the reaction conditions (the reaction temperature is 400 °C). In contrast, the generation of **P16** is irreversible because the reverse reaction has an activation free energy of 45.2 kcal/mol. Consequently, the reaction does not follow our regiochemistry prediction model and the thermodynamically more stable product **P16** was obtained experimentally.

Conclusions

In summary, we report here our DFT understanding of the mechanism and regioselectivity of intramolecular [2+2] cycloaddition of ene–ketenes. Our calculations indicate that both normal and cross-[2+2] cycloadditions are concerted processes. The normal [2+2] cycloaddition transition state is generating an internal carbocation while the cross-[2+2] cycloaddition transition state is forming an external carbocation (Scheme 1). Both the tether and the substituent(s) on the alkene affect the relative stability of these carbocations, which consequently determines the regiochemistry of intramolecular [2+2] cycloadditions. For example, the terminal ene–ketene favors normal [2+2] cycloaddition because the corresponding transition state is generating a secondary carbocation whereas the transition state in the cross-[2+2] cycloaddition pathway is forming a primary carbocation. In contrast, an ene–ketene with two terminal substituents favors the cross-[2+2] cycloaddition because its transition state is leading to a tertiary carbocation, while the normal [2+2] cycloaddition transition state is forming a less stable secondary carbocation. Our regiochemistry prediction model can also be applied to several ene–ketenes with different tethers. We believe that such an understanding would help chemists understand the previously reported reactions, and design new [2+2] cycloadditions to synthesize four-membered carbocycles.

Computational Methods

All calculations were performed with the Gaussian 09 program.[13] Geometry optimizations of all the minima and transition states involved were carried out using the B3LYP[14] functional and the def2-SVP[15] basis set in the gas phase. Frequency calculations at the same level were carried out to confirm each stationary point to be either a minimum or a transition state. Intrinsic reaction coordinate (IRC)[16] calculations were applied to confirm the connection of each transition state to its corresponding reactant and product for many of the reactions studied here (local quadratic approximation was used for increasing the steps of IRC calculations). All possible conformers for substrates, products, and transition states have been searched and located (by adjusting their relative orientations of different functional groups manually), but only the most stable ones were reported. ωB97XD functional[17] and def2-TZVPP[15] basis set were used for single-point energy calculations in toluene (SMD solvation model[18]) based on the optimized structures at the B3LYP/def2-SVP level. The ωB97XD functional was found to give the

most accurate kinetic and thermodynamic data as compared to the CCSD(T)/cc-pVTZ calculations of the model reactions (see Supporting Information for details).[19,20] All figures of 3D structures were prepared with CYLview.[21] Frontier molecular orbitals computed at the B3LYP/def2-SVP level were visualized with VMD.[22]

[1] a) T. T. Tidwell, *Eur. J. Org. Chem.* **2006**, 563–576; b) A. D. Allen, T. T. Tidwell, *Chem. Rev.* **2013**, *113*, 7287–7342; c) B. B. Snider, *Chem. Rev.* **1988**, *88*, 793–811; d) C. M. Rasik, M. K. Brown, *Synlett* **2014**, *25*, 760–765.

[2] a) N. H. Vo, B. B. Snider, *J. Org. Chem.* **1994**, *59*, 5419–5423; b) Q. Wang, C. Chen, *Org. Lett.* **2008**, *10*, 1223–1226; c) X. Wu, H.-J. Wang, Y.-S. Huang, W.-D. Z. Li, *Org. Lett.* **2018**, *20*, 1871–1874.

[3] a) C.-H. Jun, *Chem. Soc. Rev.* **2004**, *33*, 610–618; b) L. Souillart, N. Cramer, *Chem. Rev.* **2015**, *115*, 9410–9464; c) P.-h. Chen, G. Dong, *Chem. Eur. J.* **2016**, *22*, 18290–18315; d) P.-h. Chen, B. A. Billett, T. Tsukamoto, G. Dong, *ACS Catal.* **2017**, *7*, 1340–1360.

[4] a) D. J. Pasto, *J. Am. Chem. Soc.* **1979**, *101*, 37–46; b) L. A. Burke, *J. Org. Chem.* **1985**, *50*, 3149–3155; c) X. Wang, K. N. Houk, *J. Am. Chem. Soc.* **1990**, *112*, 1754–1756; d) F. Bernardi, A. Bottoni, M. A. Robb, A. Venturini, *J. Am. Chem. Soc.* **1990**, *112*, 2106–2114; e) E. Valenti, M. A. Pericas, A. A. Moyano, *J. Org. Chem.* **1990**, *55*, 3582–3593; f) S. Yamabe, K. Kuwata, T. Minato, *Theor. Chem. Acc.* **1999**, *102*, 139–146; g) B. R. Ussing, C. Hang, D. A. Singleton, *J. Am. Chem. Soc.* **2006**, *128*, 7594–7607; h) Y. Wang, D. Wei, Z. Li, Y. Zhu, M. Tang, *J. Phys. Chem. A* **2014**, *118*, 4288–4300.

[5] a) I. Marko, B. Ronsmans, A.-M. Hesbain-Frisque, S. Dumas, L. Ghosez, B. Ernst, H. Greuter, *J. Am. Chem. Soc.* **1985**, *107*, 2192–2194; b) B. B. Snider, R. A. H. F. Hui, Y. S. Kulkarni, *J. Am. Chem. Soc.* **1985**, *107*, 2194–2196; c) B. B. Snider, R. A. H. F. Hui, *J. Org. Chem.* **1985**, *50*, 5167–5176; d) B. B. Snider, A. J. Allentoff, M. B. Walner, *Tetrahedron* **1990**, *46*, 8031–8042; e) W. T. Brady, Y. F. Giang, *J. Org. Chem.* **1985**, *50*, 5177–5179; f) W. T. Brady, Y. Q. Gu, *J. Org. Chem.* **1988**, *53*, 1353–1356; g) F. Arya, J. Bouquant, J. Chuche, *Tetrahedron Lett.* **1986**, *27*, 1913–1914.

[6] B.-S. Li, B.-M. Yang, S.-H. Wang, Y.-Q. Zhang, X.-P. Cao, Y.-Q. Tu, *Chem. Sci.* **2012**, *3*, 1975–1979.

[7] a) V. Tran, T. G. Minehan, *Org. Lett.* **2011**, *13*, 6588–6591; b) S. L. Xu, H. W. Moore, *J. Org. Chem.* **1989**, *54*, 6018–6021; c) S. L. Xu, H. W. Moore, *J. Org. Chem.* **1991**, *56*, 6094–6103.

[8] K. L. McCaleb, R. L. Halcomb, *Org. Lett.* **2000**, *2*, 2631–2634.

[9] a) G. Ramírez-Galicia, M. F. Rubio, F. Jiménez-Cruz, *THEOCHEM* **2006**, *773*, 53–58; b) M. F. Rubio, F. Jiménez-Cruz, G. Ramírez-Galicia, *J. Mex. Chem. Soc.* **2010**, *54*, 209–215; c) M. Zahedifar, H. Sheibani, V. Saheb, *Synlett* **2018**, *29*, 1836–1841.

[10] G.-J. Jiang, Y. Wang, Z.-X. Yu, *J. Org. Chem.* **2013**, *78*, 6947–6955.

[11] a) S. W. Baldwin, E. H. Page Jr., *J. Chem. Soc., Chem. Commun.* **1972**, 1337–1338; b) B. B. Snider, Y. S. Kulkarni, *J. Org. Chem.* **1987**, *52*, 307–310; c) B. B. Snider, M. Walner, *Tetrahedron* **1989**, *45*, 3171–3182; d) B. B. Snider, A. J. Allentoff, Y. S. Kulkarni, *J. Org. Chem.* **1988**, *53*, 5320–5328.

[12] a) R. M. Beesley, C. K. Ingold, J. F. Thorpe, *J. Chem. Soc.* **1915**, *107*, 1080–1106; b) C. K. Ingold, *J. Chem. Soc.* **1921**, *119*, 305–329.

[13] M. J. Frisch, G. W. Trucks, H. B. Schlegel, G. E. Scuseria, M. A. Robb, J. R. Cheeseman, G. Scalmani, V. Barone, B. Mennucci, G. A. Petersson, H. Nakatsuji, M. Caricato, X. Li, H. P. Hratchian, A. F. Izmaylov, J. Bloino, G. Zheng, J. L. Sonnenberg, M. Hada, M. Ehara, K. Toyota, R. Fukuda, J. Hasegawa, M. Ishida, T. Nakajima, Y. Honda, O. Kitao, H. Nakai, T. Vreven, J. A. Montgomery Jr., J. E. Peralta, F. Ogliaro, M. Bearpark, J. J. Heyd, E. Brothers, K. N. Kudin, V. N. Staroverov, R. Kobayashi, J. Normand, K. Raghavachari, A. Rendell, J. C. Burant, S. S. Iyengar, J. Tomasi, M. Cossi, N. Rega,

J. M. Millam, M. Klene, J. E. Knox, J. B. Cross, V. Bakken, C. Adamo, J. Jaramillo, R. Gomperts, R. E. Stratmann, O. Yazyev, A. J. Austin, R. Cammi, C. Pomelli, J. W. Ochterski, R. L. Martin, K. Morokuma, V. G. Zakrzewski, G. A. Voth, P. Salvador, J. J. Dannenberg, S. Dapprich, A. D. Daniels, Ö. Farkas, J. B. Foresman, J. V. Ortiz, J. Cioslowski, D. J. Fox, *Gaussian 09, Revision E.01*, Gaussian, Inc., Wallingford CT, **2013**.

[14] a) A. D. Becke, *J. Chem. Phys.* **1993**, *98*, 5648–5652; b) C. Lee, W. Yang, R. G. Parr, *Phys. Rev. B* **1988**, *37*, 785–789.

[15] F. Weigend, R. Ahlrichs, *Phys. Chem. Chem. Phys.* **2005**, *7*, 3297–3305.

[16] K. Fukui, *Acc. Chem. Res.* **1981**, *14*, 363–368.

[17] J.-D. Chai, M. Head-Gordon, *Phys. Chem. Chem. Phys.* **2008**, *10*, 6615–6620.

[18] A. V. Marenich, C. J. Cramer, D. G. Truhlar, *J. Phys. Chem. B* **2009**, *113*, 6378–6396.

[19] G. D. Purvis III, R. J. Bartlett, *J. Chem. Phys.* **1982**, *76*, 1910–1918.

[20] T. H. Dunning Jr., *J. Chem. Phys.* **1989**, *90*, 1007–1023.

[21] C. Y. Legault, CYLview, 1.0b; Université de Sherbrooke, **2009**. http://www.cylview.org.

[22] W. Humphrey, A. Dalke, K. Schulten, *J. Mol. Graphics* **1996**, *14*, 33–38.